Article

Discovery Medicine 2026; 38(210): 2231–2251
https://doi.org/10.24976/Discov.Med.202638210.175

Surface Matrix Electrode Array-Guided Recurrent Laryngeal Nerve Mapping Without Nerve Exposure: A Rabbit Proof-of-Concept Pilot Study

Jialong Wu[1,2], Wenqing Hu[3], Jie Hao[3], Tao Li[1], Fengwu Tan[1], Xiaohong Chen[1,4,5,*]

[1]Department of Otolaryngology Head and Neck Surgery, The Second Affiliated Hospital of Anhui Medical University, 230601 Hefei, Anhui, China
[2]Department of Otolaryngology, Head and Neck Surgery, The First Hospital of Qinhuangdao, 066000 Qinhuangdao, Hebei, China
[3]National Engineering Research Center for Application Specific Integrated Circuit Design, Institute of Automation, Chinese Academy of Sciences (CASIA), 100190 Beijing, China
[4]Department of Otolaryngology, Head and Neck Surgery, Beijing Tongren Hospital, Capital Medical University, 100730 Beijing, China
[5]Key Laboratory of Otolaryngology, Head and Neck Surgery (Capital Medical University), Ministry of Education, 100730 Beijing, China
*Correspondence: trchxh@163.com (Xiaohong Chen)
Submitted: 25 March 2026 Revised: 14 May 2026 Accepted: 3 June 2026 Published: 23 July 2026

Background: Precise recurrent laryngeal nerve (RLN) localization remains challenging in thyroid surgery, particularly in re-operative cases where peri-neural fibrosis distorts anatomy and limits conventional single-point neural monitoring. We aimed to design, optimize stimulation parameters for, and preliminarily evaluate the feasibility of a surface matrix electrode array guide for structured RLN mapping under a skin-incision-only, nerve-unexposed condition.

Methods: Nine New Zealand White rabbits were assigned to first-, second-, and third-operation groups to model progressive peri-neural fibrosis. A 10 × 10 mm flexible array guide with a 5 × 5 matrix of 25 stimulation sites (2.0 mm spacing) was applied to paratracheal soft tissue under a skin-incision-only condition (18 sides; 90 accuracy assessments). Localization accuracy was defined as electrophysiological reference point-to-nerve distance ≤2 mm, using the surgically exposed RLN as the reference standard.

Results: Effective stimulation distance was 1–2 mm at 0.5 mA and 4–5 mm at 1.0 mA, justifying the 2.0 mm inter-site spacing and 0.5 mA working current. Overall descriptive site-level localization accuracy was 92.2% (83/90 sites). The array guide consistently reconstructed the RLN trajectory across all 18 evaluated sides, with similar descriptive accuracy between the left and right sides. Seven initially false-negative sites in re-operative animals were recovered by increasing the stimulation current to 0.8–1.0 mA. One case of an anomalous RLN course with lateral displacement toward the carotid sheath was successfully identified without prior anatomical assumptions.

Conclusions: These preliminary findings provide the electrophysiological rationale and initial accuracy data necessary to justify progression to large-animal validation studies, representing a required step prior to clinical translation. Given the small sample size, rabbit model anatomy, and mild-to-moderate fibrosis burden, these findings should be interpreted as hypothesis-generating and are not directly extrapolable to clinical practice without further large-animal validation.

Keywords: recurrent laryngeal nerve; intraoperative neural monitoring; electrode array; nerve mapping; thyroid surgery; re-operative thyroid surgery; peri-neural fibrosis

Introduction

Recurrent laryngeal nerve (RLN) injury remains one of the most serious and clinically significant complications of thyroid surgery [1]. The nerve governs all intrinsic laryngeal musculature except the cricothyroid, and its disruption produces a clinical spectrum ranging from dysphonia, dysphagia, and aspiration to life-threatening airway compromise in bilateral vocal fold paralysis [2,3]. Despite progressive refinement of surgical technique and deepening anatomical knowledge, RLN injury remains clinically relevant after thyroid surgery, with a reported incidence ranging from 4.3% in surgery for a single nodule to 9.0% in surgery for differentiated thyroid cancer; the risk increases further in the re-operative setting [4]. These figures, drawn from large multicenter series, have remained largely unchanged over the past two decades, which is a sobering indication that anatomical dissection alone is insufficient to guarantee nerve preservation in every case.

The introduction of intraoperative neural monitoring (IONM) represented a conceptual advance. By coupling electrical stimulation with real-time electromyographic (EMG) recording from the vocal cord musculature, IONM enables the surgeon to identify the RLN/vagus nerve before or during dissection, detect impending injury through adverse signal change, and document intact neural func-

tion at the conclusion of the procedure [5,6,7]. Guidelines from the International Neural Monitoring Study Group have standardized the use of IONM and established it as an adjunct to the gold standard of visual nerve identification in thyroid surgery; furthermore, its adoption has grown steadily across surgical centers worldwide [8,9]. Yet conventional IONM, particularly intermittent IONM, is fundamentally a single-point, surgeon-directed interrogation tool. A handheld probe is applied to a suspected nerve location to deliver on-demand stimulation, and the resulting EMG response is interpreted, often first in terms of signal presence or loss, but more formally through changes in amplitude, latency, waveform, and loss of signal [10,11]. Spatial information must be inferred through sequential, surgeon-directed point-by-point exploration with a handheld probe, an operator-dependent process that becomes especially challenging in the re-operative field, where scarring, fibrosis, and distortion of landmarks may displace or obscure the RLN [11,12].

The re-operative scenario deserves particular consideration, as peri-neural scarring and anatomy distortion can displace the RLN, complicate EMG interpretation, and increase the risk of false-negative localization or inadvertent nerve injury during single-point exploration [7,11,13,14]. Several technical strategies have been proposed to address this challenge. Continuous vagal stimulation during dissection provides real-time traction alerts but does not enable pre-dissection nerve localization [8,15,16,17]. Ultrasound-guided identification has demonstrated promise but requires dedicated imaging infrastructure and operator expertise [14,18,19]. Image-guided and augmented-reality navigation systems have been described but remain limited by workflow complexity and registration demands [20,21]. A simple, broadly applicable method for explicit topographic localization of the RLN before wide nerve exposure has not yet been established [22].

The concept underlying the present work is straightforward. If the current–distance behavior of a monopolar probe is characterized, a structured array of stimulation sites can be used to generate a spatial EMG response pattern that may assist inference of the nerve's position and course [8,23]. Within a transverse row, the site eliciting the highest EMG amplitude is expected to lie closest to the RLN trunk or one of its major motor branches, although this inference is influenced by current dispersion, tissue impedance, and local branching anatomy [11,23]. Connecting these electrophysiological reference points along the craniocaudal axis reconstructs the nerve's course as a continuous trajectory [8]. No anatomical assumption is required; the nerve is localized by its own electrical signature.

We report here the design, parameter optimization, and proof-of-concept validation of a surface matrix electrode array guide implementing this principle, evaluated in nine New Zealand White rabbits across three progressive surgical groups designed to model increasing peri-neural fibrosis. Localization accuracy was assessed using the surgically exposed nerve as the anatomical reference standard. The results provide preliminary evidence supporting the feasibility of this method and the rationale of electrophysiological parameters underlying its potential translation to the clinical setting.

Materials and Methods

This study was designed as a preliminary, exploratory, proof-of-concept investigation to assess the feasibility and basic electrophysiological rationale of the array-guide method prior to formal power-calculated studies. Accordingly, sample sizes were determined by practical and ethical constraints of the pilot design rather than by formal power analysis, and findings should be interpreted as hypothesis-generating rather than confirmatory.

Experimental Animals

This study was conducted in three experimental series between May and August 2024 using a total of 9 healthy adult New Zealand White rabbits (either sex; body weight: 3.5–4.5 kg; Suibei Laboratory Animal Breeding Farm, Guangzhou, China; license no. SCXK(Yue)2020-0050). All procedures were approved by the Institutional Animal Care and Use Committee of Laboratory Animal Sciences, Chinese Academy of Medical Sciences (approval no. KR-IACUC-T-2024-011) and performed in accordance with the Guide for the Care and Use of Laboratory Animals and the 3R principles. Animals were housed under standard specific pathogen-free (SPF) conditions (temperature 18–22 °C; humidity 50 ± 5%; 12 h light/dark cycle) with ad libitum access to food and water and acclimatized for one week before each experiment.

This study employed a longitudinal within-animal repeated-surgery design rather than three independent cohorts. The same animals underwent successive neck surgeries at approximately one-month intervals. Each animal contributed data from the surgical stage(s) completed before reaching a humane endpoint or being lost to follow-up. Accordingly, the three experimental series represent sequential time points in the same animals rather than independent groups: Series 1 (29 May 2024; first operation; rabbits B01–B09, n = 9); Series 2 (1 July 2024; second operation; rabbits B01–B07, n = 7); and Series 3 (1 August 2024; third operation; rabbits B01, B03, B04, n = 3). The interval between successive surgeries was 28–35 days. Absorbable sutures were used in Series 2 and non-absorbable buried sutures in Series 3 to generate differing degrees of peri-neural fibrosis. The overall allocation of animals across the three surgical series, including criteria-based exclusions and data contributions of each animal to the analyses reported below, is summarized in Fig. 1.

Animals were eligible to proceed to the next scheduled surgery only if they met all of the following criteria at the end of the 28–35-day post-operative observation period:

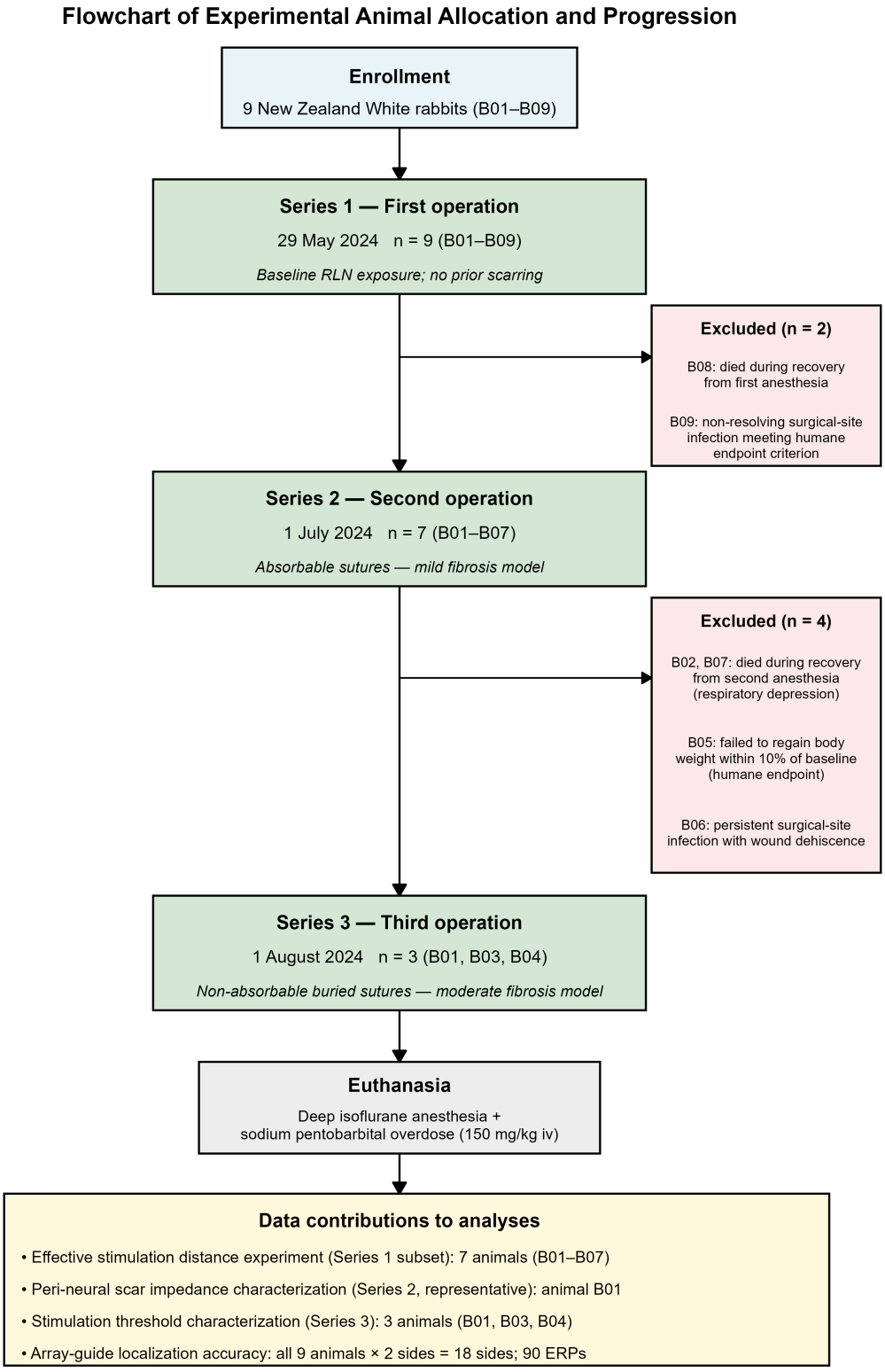

Fig. 1. Flowchart of experimental animal allocation and progression. Flow diagram summarizing the longitudinal within-animal repeated-surgery design, with criteria-based exclusions and contributions of each animal to the analyses reported in the Results. Nine New Zealand White rabbits (B01–B09) were enrolled and underwent up to three successive cervical surgeries at 28–35-day intervals. Animals were eligible to proceed to the subsequent surgery only if pre-specified clinical criteria were met. Exclusions and corresponding reasons are shown in the side branches. The lower panel summarizes the contribution of each surgical series to the individual analyses reported in the Results. ERP, electrophysiological reference point; iv, intravenous; RLN, recurrent laryngeal nerve.

(1) Uneventful recovery from anesthesia, with resumption of normal feeding, drinking, and activity within 48 h post-operatively.

(2) Body weight maintained within 10% of pre-operative baseline by the day of re-operation.

(3) Absence of surgical-site infection, wound dehiscence, or respiratory distress.

(4) No observable voice change, inspiratory stridor, or feeding difficulty suggestive of iatrogenic RLN injury on the preceding side.

(5) General clinical score consistent with normal welfare under institutional veterinary assessment.

Animals not meeting any of these criteria were excluded from subsequent surgery and humanely euthanized. Between Series 1 and Series 2, two animals were excluded. B08 died during recovery from the first anesthesia, and B09 developed a non-resolving surgical-site infection that met the humane endpoint criterion. Between Series 2 and Series 3, four animals were excluded. B02 and B07 died during recovery from the second anesthesia, attributed to respiratory depression unresponsive to resuscitation. B05 failed to regain body weight to within 10% of pre-operative baseline by post-operative day 30, meeting the pre-specified humane endpoint criterion. B06 had persistent surgical-site infection with wound dehiscence that did not resolve under standard veterinary care.

At the end of the assigned surgical series (i.e., after the final operation scheduled for each animal) or upon reaching a predefined humane endpoint, animals were euthanized under deep isoflurane anesthesia by intravenous overdose of sodium pentobarbital (150 mg/kg; catalog no. P3761; Sigma-Aldrich, St. Louis, MO, USA) administered via the marginal ear vein, in accordance with the 2020 AVMA Guidelines for the Euthanasia of Animals. Death was confirmed by cessation of cardiac activity and loss of the corneal reflex.

Equipment and Monitoring System

Intraoperative neural monitoring (IONM) was performed using a NIM-Response 3.0 electromyography (EMG) monitoring system (Medtronic Xomed, Jacksonville, FL, USA), configured with a hand-held monopolar stimulation probe (tip diameter 1.0 mm; catalog no. 8220325, Medtronic Xomed, Jacksonville, FL, USA), contact surface electrodes, and a subcutaneous ground electrode (catalog no. 8227103, Medtronic Xomed, Jacksonville, FL, USA). A customized endotracheal tube was fabricated by securing a Medtronic standard contact electrode (catalog no. 8253365, Medtronic Xomed, Jacksonville, FL, USA) to the lateral wall of an animal-grade endotracheal tube (2.5 mm inner diameter; Anhui Tiankang Medical, Xuancheng, China), ensuring tight apposition of recording contacts against bilateral vocal cord musculature after intubation. EMG signal parameters, peak amplitude (μV) and latency (ms), were displayed in real time and saved digitally for post-hoc analysis (Fig. 2A). Additional equipment included a veterinary laryngoscope (VM-100; Hangzhou Haoke Medical Instruments, Hangzhou, China), a small-animal ventilator (model DH-150; RWD Life Science, Shenzhen, China), a thermostatic operating table maintained at 36–38 ℃ (model KT-1000; Beijing Ketai Hengsheng Technology, Beijing, China), and a microsurgical instrument set including vessel forceps, micro-scissors, and needle holders (Shanghai Medical Instruments, Shanghai, China).

Array Guide: Design Rationale and Fabrication

Array guide design was prospectively informed by the effective stimulation distance experiment conducted in Series 1 animals (the Effective Stimulation Distance: Preliminary Experiment), which directly determined the inter-site spacing and working current. Stimulation threshold characterization (the Stimulation Threshold of the RLN and Vagus Nerve subsection) was subsequently performed in Series 3 animals as an independent electrophysiological validation of the selected parameters, rather than a prospective design input.

Effective Stimulation Distance: Preliminary Experiment

The choice of current intensities tested in this preliminary experiment was guided by the established clinical literature on intraoperative neural monitoring. The International Neural Monitoring Study Group (INMSG) guidelines recommend a stimulation current of 1–2 mA for routine RLN and vagus nerve (VN) identification and a lower current (approximately 0.5 mA) for nerve mapping, where the objective is to localize the nerve trunk with higher spatial specificity rather than merely to confirm its functional integrity [8,11]. Because the present array-guide method is intended specifically for topographic localization rather than functional confirmation, 0.5 mA was prospectively selected as the candidate lower-bound working current, and the empirical experiment was designed to test whether this current would indeed provide an effective stimulation radius compatible with a practical inter-site spacing and with safe, selective activation of the RLN. Higher stimulation currents (up to 2.5 mA) were also tested to characterize the full current-distance relationship and to establish an upper reference limit for situations in which compensation for scar-related impedance may be required in re-operative cases.

Before fabricating the array guide, a preliminary experiment was performed in a subset of rabbits from Series 1 (n = 7; animals B01–B07) to empirically determine the effective lateral stimulation distance of the monopolar probe at different current intensities. This preliminary experiment was conducted at the beginning of the Series 1 surgical day (29 May 2024), and array design parameters were finalized before the subsequent surgical procedures performed later that day. Animals B08 and B09, operated later on the

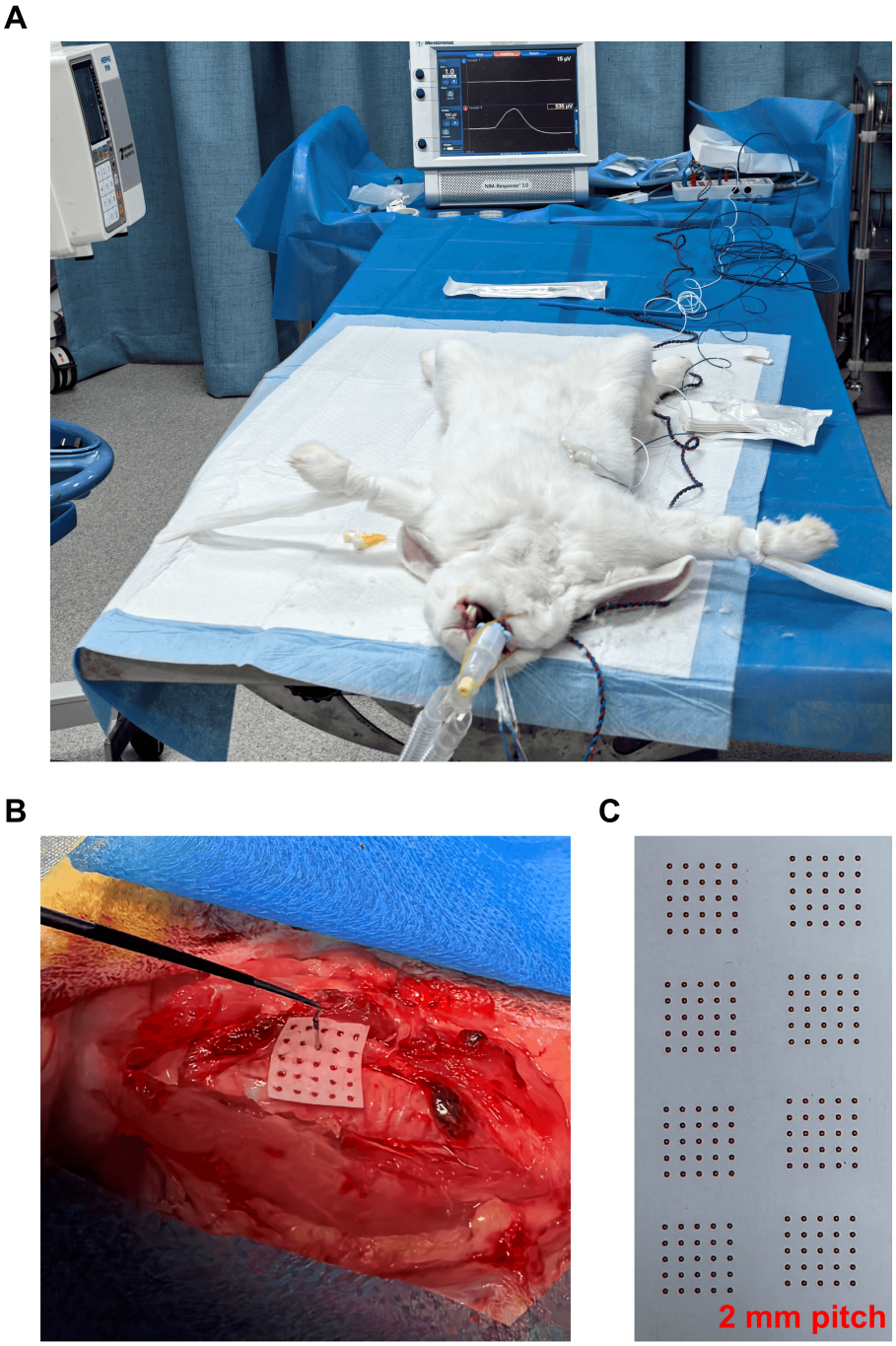

Fig. 2. Experimental setup and array guide. (A) Intraoperative overview photograph showing the rabbit positioned supine with the NIM-Response 3.0 system (background), customized endotracheal tube electrodes (connected to vocal cords), and subcutaneous ground electrode. (B) Close-up intraoperative photograph showing the hand-held stimulation probe positioned at a numbered site on the array guide, which is applied to the paratracheal soft tissue. (C) Photograph of the array guide. The 5 × 5 matrix of 25 stimulation sites (numbered 1–25; 0.5-mm diameter holes; 2.0 mm inter-site spacing) is visible.

same day after the array parameters had been established, did not undergo this distance-characterization protocol but contributed array-guided localization data at their first operation (the Array-Guide Localization Procedure). Of these seven, four animals (B02–B05) yielded recording sessions meeting the pre-specified quality criterion of plateau amplitude ≥500 μV under direct nerve-surface stimulation (the same criterion subsequently applied to the left-side RLN session of B04 in Table 1). The remaining three animals (B01, B06, B07) did not meet this contact-quality criterion in this experiment and were excluded prospectively. Their data are not included in Fig. 3B or in the cohort-level effective-stimulation-radius estimates reported in the Results (Effective Stimulation Distance and Array Param-

Table 1. Stimulation thresholds and plateau amplitudes of the recurrent laryngeal nerve (RLN) and vagus nerve (VN) for representative animals (August 2024 cohort).

Animal	Nerve	Side	Min threshold (mA)	Plateau onset (mA)	Peak amplitude at plateau (μV)
B01	*RLN*	Right	0.20	0.30	1494–1561
B03	*RLN*	Right	0.20	0.30	800–1073
B04	*RLN*	Right	0.08	0.10	1065–1782
B04	*VN*	Right	0.10	0.30	992–1463
B01	*VN*	Right	0.30	0.40	1208–1299

Data represent individual recording sessions. Amplitude ranges reflect three consecutive stimulations at plateau current. All recordings were performed on the right side, which was the pre-specified standardized primary recording site in this protocol (see the Materials and Methods, Stimulation Threshold of the RLN and Vagus Nerve). Left-side RLN recording was attempted only in animal B04 as a time-permitting additional session. No left-side recordings were attempted in B01 or B03. Data from the left RLN of animal B04 are not included in this table because the plateau amplitude at this recording site (278–324 μV) fell below the pre-specified representativeness threshold of 500 μV, despite a low stimulation threshold of 0.05 mA. This pattern is diagnostic of suboptimal electrode-to-vocal cord contact rather than intrinsic nerve pathology and is consistent with the normal plateau amplitude observed contralaterally in the same animal (right RLN of B04; 1065–1782 μV). Vagus nerve threshold data for animal B03 are not included because, within the per-session recording time budget, VN characterization could not be completed after RLN characterization. This is an operational omission rather than a signal-quality exclusion. RLN, recurrent laryngeal nerve; VN, vagus nerve.

eter Rationale). After surgical exposure of the RLN, the probe tip was placed at precisely measured lateral distances from the nerve surface (0.5, 1.0, 2.0, 3.0, and 5.0 mm medially and laterally) and stimulated at 0.5, 1.0, 1.5, 2.0, and 2.5 mA. An EMG amplitude ≥100 μV was defined as a positive response.

The maximum lateral distance at which a positive response could be reliably elicited was recorded as the effective stimulation distance at each current level (Fig. 3B). The identical protocol was subsequently repeated under a skin-incision-only condition (overlying soft tissue intact, nerve not surgically exposed) to verify that array-guide stimulation would be feasible without mandatory nerve exposure. The empirical results of this experiment are reported in the Results (Effective Stimulation Distance and Array Parameter Rationale) and directly informed the final array design parameters.

Two geometric constraints guided the subsequent translation of this current-distance relationship into an array design. The first constraint concerns the avoidance of blind zones, that is, locations within the array footprint where no stimulation site could elicit a detectable response from an underlying nerve. For a square grid with an inter-site spacing of s, the point most distant from any stimulation site lies at the center of the square formed by four adjacent sites. This worst-case distance equals half of the square's diagonal, i.e., approximately 0.71 × s ($\sqrt{2} \times s/2$). To ensure that such a point still lies within reach of at least one stimulation site, the effective stimulation radius at the working current must satisfy effective radius ≥0.71 × s. For an inter-site spacing of 2 mm, this corresponds to a minimum required radius of approximately 1.4 mm. The second constraint concerns the avoidance of cross-activation, that is simultaneous activation of the underlying nerve from multiple non-adjacent stimulation sites, which would preclude identification of the single site closest to the nerve. To preserve this discrimination, the effective stimulation radius must not substantially exceed the inter-site spacing, i.e., the effective radius should be ≤s. For a 2-mm spacing, this upper limit is approximately 2 mm. Both constraints are simultaneously satisfied when the effective stimulation radius lies in the approximate range of 1.4–2 mm. The empirically observed radius at 0.5 mA (the Results, Effective Stimulation Distance and Array Parameter Rationale) reached the 2-mm upper limit of this window in most recording sessions, comfortably satisfying the cross-activation constraint. In a subset of sessions, the effective radius approached the lower bound (~1 mm), which in the strict geometric worst case would leave a small region at the center of four adjacent sites unstimulated. However, because the RLN extends as a continuous longitudinal structure rather than a point, any nerve segment crossing the array footprint will pass within ≤1 mm of at least one stimulation site in each transverse row, and no false-negative ERPs attributable to inter-site blind zones were observed in unscarred tissue at 0.5 mA in this study (the Results, RLN Localization Accuracy of the Array Guide). The radius at 1.0 mA (4–5 mm) violates the cross-activation constraint. These geometric considerations, together with the clinical rationale above, determined the final array design parameters (2-mm inter-site spacing, 0.5 mA working current, see Array Guide Fabrication).

A

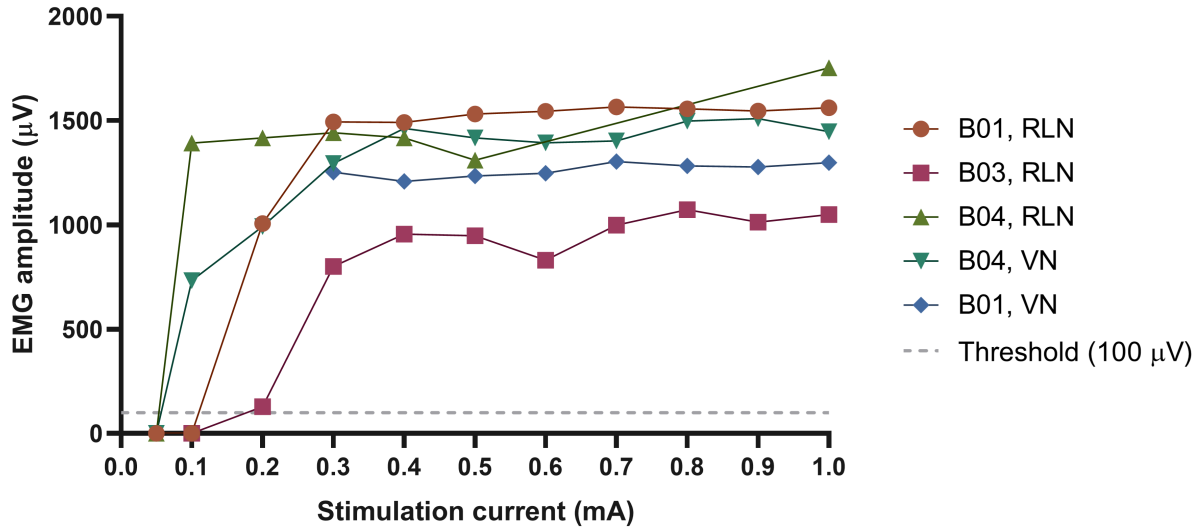
2000
1500
1000
500
0
EMG amplitude (μV)
0.0
0.1
0.2
0.3
0.4
0.5
0.6
0.7
0.8
0.9
1.0
Stimulation current (mA)
B01, RLN
B03, RLN
B04, RLN
B04, VN
B01, VN
Threshold (100 μV)

B

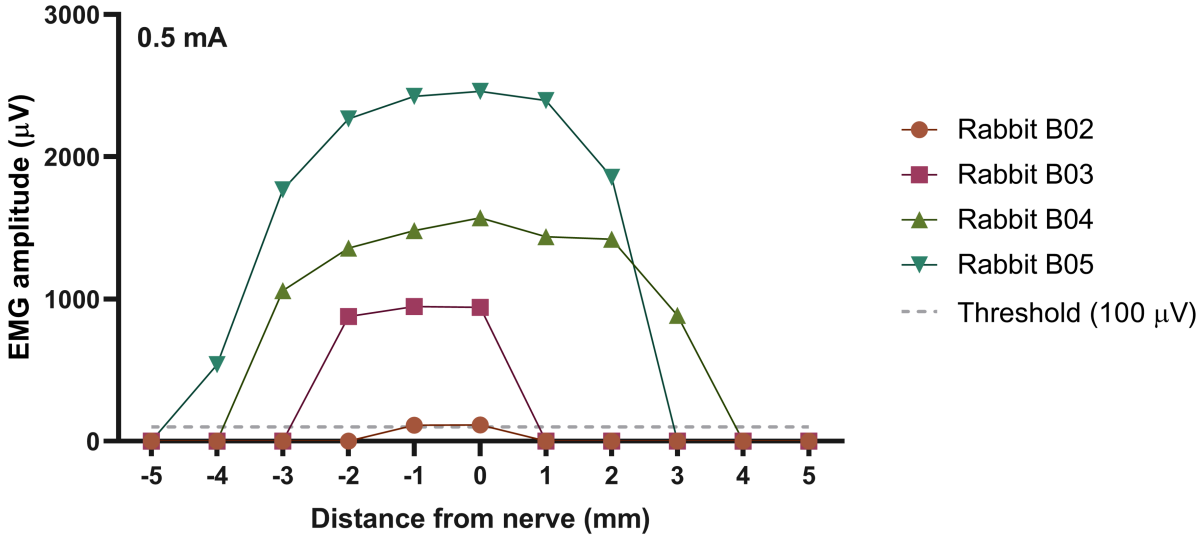
3000
2000
1000
0
0.5 mA
EMG amplitude (μV)
-5
-4
-3
-2
-1
0
1
2
3
4
5
Distance from nerve (mm)
Rabbit B02
Rabbit B03
Rabbit B04
Rabbit B05
Threshold (100 μV)

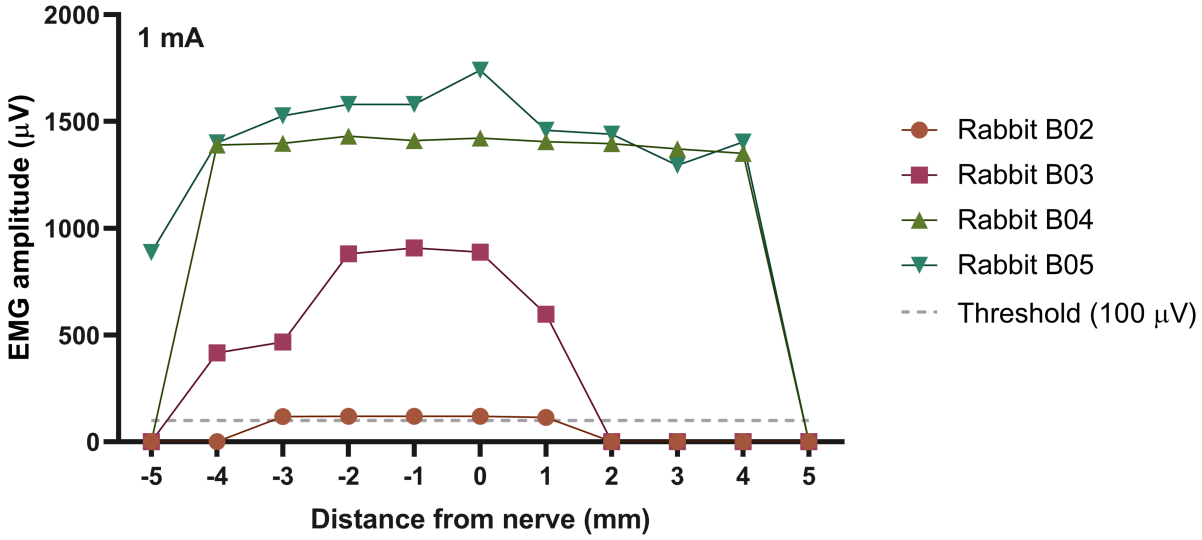
2000
1500
1000
500
0
1 mA
EMG amplitude (μV)
-5
-4
-3
-2
-1
0
1
2
3
4
5
Distance from nerve (mm)
Rabbit B02
Rabbit B03
Rabbit B04
Rabbit B05
Threshold (100 μV)

Fig. 3. Stimulation parameter validation. (A) Electromyographic (EMG) amplitude (μV) as a function of stimulation current (0.05–1.0 mA) for the recurrent laryngeal nerve (RLN) and vagus nerve (VN) in five representative recording sessions (animals B01, B03, B04). The five curves correspond, one-to-one, to the five rows of Table 1 (in the order tabulated). B01 right RLN, B03 right RLN, B04 right RLN, B04 right VN, B01 right VN. The right side was the pre-specified standardized primary recording side in this protocol (the Materials and Methods, Stimulation Threshold of the RLN and Vagus Nerve). The single attempted left-side session (B04 left RLN) was excluded due to anomalously low plateau amplitude (278–324 μV), likely attributable to suboptimal electrode-to-vocal cord contact rather than intrinsic nerve pathology, as supported by the normal plateau amplitude on the contralateral right RLN of the same animal. Lines are not interpolated across untested current levels. (B) Effective stimulation distance at 0.5 mA (upper panel) and 1.0 mA (lower panel). Each data point represents mean EMG amplitude (μV) at a given lateral distance from the nerve surface (mm). The x-axis represents the lateral distance from the nerve surface (mm); values to the left of 0 indicate positions lateral to the nerve (away from the trachea), and values to the right of 0 indicate positions medial to the nerve (toward the trachea); 0 indicates the probe positioned directly on the nerve surface. Each curve represents an individual animal recording for the four Series 1 animals (B02–B05) whose sessions met the pre-specified plateau-amplitude quality criterion described in the Materials and Methods (Effective Stimulation Distance: Preliminary Experiment). Sessions from B01, B06, and B07 were excluded prospectively for not meeting this contact-quality criterion. The absolute amplitudes recorded from animal B02 in this session were lower than those of the other three displayed animals, attributable to partial endotracheal tube electrode contact in this particular recording session rather than a property of the animal's nerve, as the same animal yielded normal supra-threshold amplitudes (~2200 μV at 1.0 mA) in a subsequent recording session with a freshly placed endotracheal tube electrode (**Supplementary Table 1a**). The shape of the B02 curve was directionally concordant with the other animals, and B02 was therefore retained in the figure on the principle of full data transparency. At 0.5 mA, the empirical amplitude maximum within an individual animal does not necessarily occur exactly at the 0 mm position. At near-threshold currents, modest sub-millimetre off-axis positions may yield equal or marginally higher responses because the recurrent laryngeal nerve is a cylindrical structure of finite caliber and the recruited motor fascicles lie at varying depths and lateral positions beneath the surface. This positional sensitivity was greatly attenuated at 1.0 mA (lower panel), where the distance-amplitude relationship exhibited a monotonic decrease with distance in each animal. The 1–2 mm effective radius at 0.5 mA was matched to the 2-mm inter-site spacing of the array guide to simultaneously minimize blind zones and cross-activation; see the Materials and Methods (Effective Stimulation Distance: Preliminary Experiment) for the geometric derivation.

Stimulation Threshold of the RLN and Vagus Nerve

To confirm that 0.5 mA reliably activates the RLN while remaining selective (i.e., not excessively over-driving the vagus nerve [VN]), threshold characterization was performed as a supplementary validation experiment in 3 animals from the August 2024 cohort (Series 3; animals B01, B03, B04). This experiment was conducted after the array design parameters had been established based on the Series 1 effective stimulation distance data (the Effective Stimulation Distance: Preliminary Experiment), and serves as an electrophysiological verification of the selected working current rather than a prospective design input. Because the primary aim of this experiment was to verify reliable and selective activation of the RLN at the candidate working current rather than to compare left and right sides, the pre-specified recording protocol targeted the right RLN as the standardized primary recording site in each animal, with the right VN additionally sampled where remaining recording time permitted. The right side was chosen as the standardized primary side for three reasons. The midline cervical approach used in this study exposes the right RLN first at each procedure, permitting standardized timing of electrode placement relative to nerve exposure. Use of a single standardized recording side across animals facilitates direct inter-animal comparison of threshold and plateau amplitudes. The per-session recording time was constrained by the need to complete array-guide localization (the Array-Guide Localization Procedure) and other assessments within a single anesthesia episode, and systematic bilateral characterization was therefore not feasible within this pilot design. Left-side RLN recording was attempted only in animal B04, in which recording time permitted an additional contralateral session. No left-side recordings were attempted in B01 or B03. The left-side session in B04 was subsequently excluded from the representative threshold-amplitude profile per the pre-specified amplitude criterion. The stimulation threshold was defined as the minimum current eliciting an EMG amplitude ≥100 μV; the current at which the amplitude stabilized (plateau) was also recorded. Representative data from the August 2024 cohort are summarized in Table 1. For threshold-amplitude profiling, recording sessions were considered representative only if plateau amplitude exceeded 500 μV, a criterion consistent with adequate electrode-to-vocal cord contact and distinguishable from recording artefact. Sessions yielding anomalously low plateau amplitudes despite low stimulation thresholds, indicative of suboptimal electrode contact rather than intrinsic nerve pathology, as evidenced by normal contralateral recordings in the same animal, were flagged prospectively and excluded from the representative threshold-amplitude profile. One such session was identified (left RLN, animal B04; plateau amplitude 278–324 μV;

details in the Results, Stimulation Thresholds of the RLN and Vagus Nerve) and excluded accordingly.

Array Guide Fabrication

Based on the preliminary parameters described above, the array guide was fabricated from a thin medical-grade flexible polyethylene terephthalate (PET) film (0.3 mm thickness; Dongguan Jinhong Packaging, Dongguan, China) with mild adhesive properties, allowing it to conform to and remain stable on soft tissue surfaces without need for suture fixation. Guided by the anatomical distance between the tracheal sidewall and the carotid sheath in New Zealand White rabbits (approximately 10–15 mm), the guide was designed as a 10 × 10 mm plate carrying a 5 × 5 matrix of 25 stimulation sites (sites numbered 1–25 sequentially). Each site consisted of a 0.5-mm-diameter through-hole punched with a micro-biopsy punch (catalog no. BP-05F, Kai Medical, Seki, Japan) to serve as a contact portal for the probe tip. Adjacent sites were spaced 2.0 mm apart (center-to-center) in both axes. Individual guides were fabricated in batches and sterilized before use (Fig. 2C).

Surgical and Experimental Procedures

Anesthesia and Preparation

Animals were fasted for 3–4 h and withheld from water for 1 h before surgery. Atropine sulfate (0.5 mg intravenously [iv]; approval no. H32020166, Jiangsu Lianshui Pharmaceutical, Lianshui, China) was administered via the marginal ear vein 30 min before induction to reduce airway secretions. General anesthesia was induced by slow intravenous injection (rate ≤0.1 mL/10 s) of a 1:1 mixture of Zoletil 50 (tiletamine/zolazepam 50 mg/mL; Virbac, Carros, France) and xylazine hydrochloride (20 mg/mL; Jilin Huamu Animal Health Products, Changchun, China) at a combined dose of 0.1 mL/kg. Induction success was confirmed by loss of the corneal reflex and limb tone. Anesthesia was maintained with inhaled isoflurane (initial 2–3%; maintenance 1–1.5%; catalog no. R510-22, RWD Life Science, Shenzhen, China) delivered via a small-animal ventilator (tidal volume 10 mL/kg; rate 40 breaths/min; inspiratory-to-expiratory ratio [I:E] 1:2). Heart rate (target 180–220 beats per minute [bpm]) and oxygen saturation (SpO_2; ≥95%) were monitored continuously.

The animal was positioned supine on the thermostatic table with the neck extended. The neck was shaved from the mandibular angle to the sternal notch and prepared with povidone-iodine (5% w/v; Shanghai Likang Disinfectant High-Tech, Shanghai, China). The customized endotracheal tube was placed under direct laryngoscopy; correct positioning was confirmed by visual inspection of electrode-to-vocal cord apposition. A subcutaneous ground electrode was inserted beneath the xiphoid process. The NIM-Response 3.0 system was configured with an EMG threshold of 100 μV, pulse repetition rate of 4 Hz, and pulse width of 100 μs.

Surgical Exposure of the RLN

A 3–4 cm midline neck incision was made, and the strap muscles were divided by blunt dissection. The RLN was identified in the tracheoesophageal groove, medial to the carotid sheath, and carefully freed from surrounding connective tissue to serve as the anatomical reference standard. In second- and third-operation animals, the degree of peri-neural adhesion was graded immediately upon surgical exposure, prior to any dissection of the scar tissue, using a four-point ordinal scoring scheme based on three objective criteria, including the circumferential extent of scar-nerve contact (% of the nerve circumference involved), tissue plane separability (blunt vs. sharp dissection required, planes identifiable vs. obliterated), and visual identifiability of the nerve through the overlying scar. The grades were defined as follows: Grade 0 (none), no scar-nerve contact, pristine planes, nerve fully visible; Grade 1 (mild), filmy scar contacting <25% of nerve circumference, easily separated by blunt dissection, nerve outline clearly visible through the scar; Grade 2 (moderate), scar contacting 25–75% of nerve circumference, sharp dissection required but planes still identifiable, nerve partially obscured; Grade 3 (severe), dense scar circumferentially encasing >75% of nerve, sharp dissection required with planes obliterated and significant risk of nerve injury, nerve not visible until completion of dissection. Grading was performed intraoperatively by the operating surgeon according to the above criteria. The grade assigned to each surgical series is reported in the Results (Effect of Peri-Neural Scar Tissue on Electrophysiological Parameters) and indicated in Fig. 4.

Effect of Peri-Neural Scar Tissue on Electrophysiological Parameters

To characterize the electrophysiological impact of peri-neural scar on intraoperative EMG-based nerve monitoring, within-animal comparisons were performed in three of the seven Series 2 animals using two complementary paradigms, with the recurrent laryngeal nerve fully exposed in all cases. The primary comparison (rabbit B01; Table 2) used a bilateral probe-placement paradigm designed to simulate the intraoperative scenario in which the surgeon cannot place the stimulating probe directly on the nerve because of overlying scar tissue. EMG recording was assessed under two conditions: (I) unscarred reference condition: probe tip placed directly on the RLN surface of the contralateral, unscarred side, at a site with no visible scar tissue; and (II) scar-adjacent condition: probe placed on normal tissue 1–2 mm lateral to a scar-covered nerve segment on the ipsilateral side. In both conditions, stimulation was applied at 0.05, 0.06, 0.10, 0.15, 0.20, 0.25, 0.30, 0.35, 0.40, 0.45, and 0.50 mA (three repetitions per current level; mean values recorded). Amplitude and latency were compared across conditions (Table 2). This within-animal bilateral comparison was chosen to control for inter-individual variation in nerve caliber and anesthetic depth.

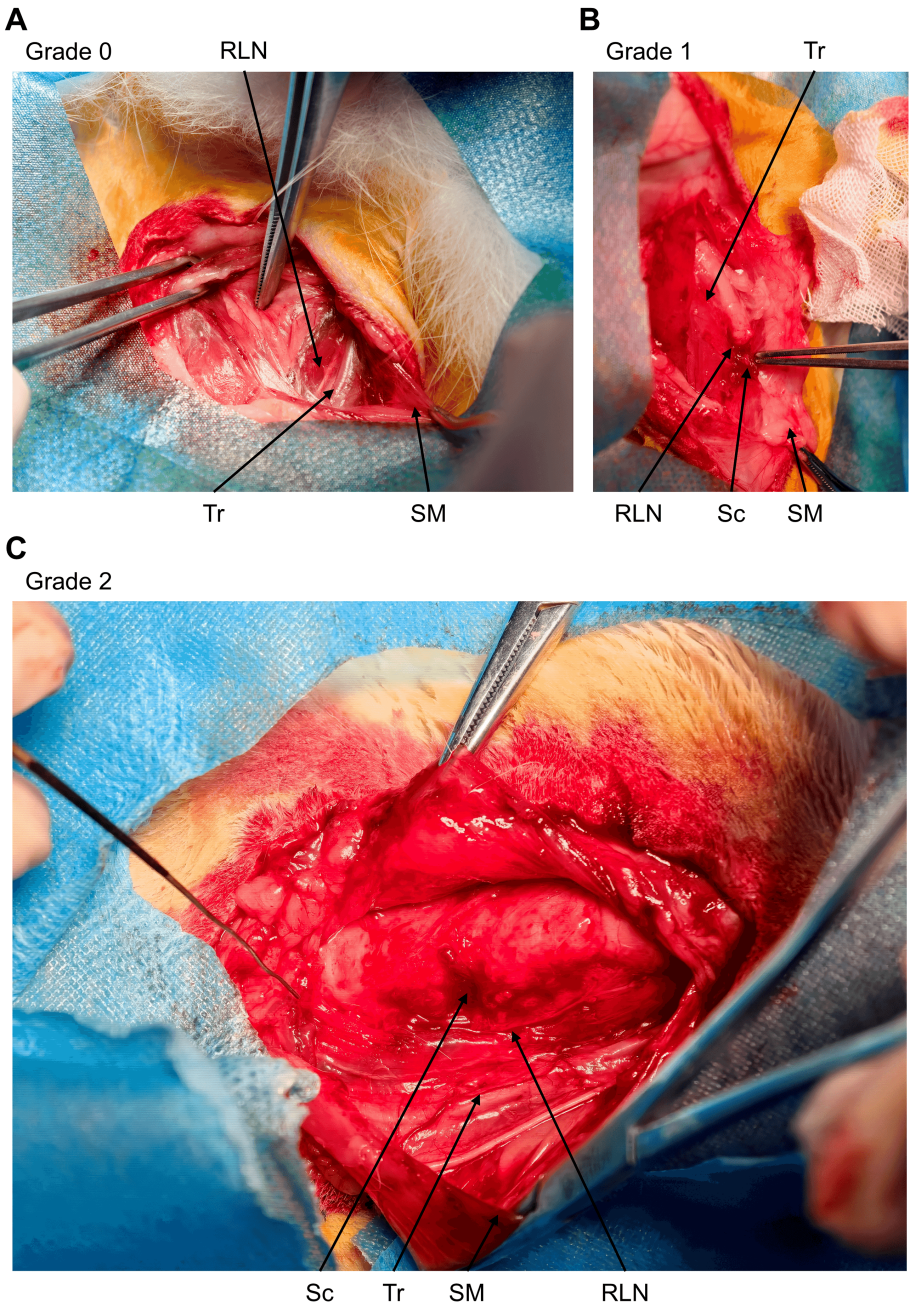

Fig. 4. Scar tissue characterization and effect on electrophysiological parameters. (A–C) Representative gross photographs of the cervical surgical field intraoperatively in the first-operation (A), second-operation (B, absorbable sutures, ~1 month), and third-operation (C, non-absorbable buried sutures, ~2 months) animals. Anatomical structures are labelled as follows. Tr, trachea; RLN, recurrent laryngeal nerve; SM, strap muscles; Sc, peri-neural scar tissue (panels B and C only). The peri-neural adhesion grade assigned to each panel according to the scheme defined in the Surgical Exposure of the RLN subsection is indicated in the upper-right corner.

Two independent supporting comparisons (rabbits B02 and B04; **Supplementary Table 1a,b**) used a sequential within-site paradigm, in which the stimulating probe was placed directly on the nerve at a scar-covered segment, and EMG responses were recorded across a stepped range of currents (0.05–2.0 mA). The overlying scar tissue was then sharply dissected from the nerve surface under microscopy, and the identical stimulation site was re-sampled across the same current range. This paradigm isolates the effect of peri-neural fibrosis on the nerve itself, eliminating both inter-side anatomical variability and any contribution of scar tissue as an interposed insulating layer between probe and nerve.

The two paradigms therefore interrogate partially distinct but clinically complementary aspects of peri-neural scar. The bilateral paradigm (B01) captures the combined

Table 2. Bilateral scar-vs-unscarred electrophysiological comparison in second-operation rabbit B01 (primary comparison).

Condition	Threshold (mA)	Amplitude at 0.5 mA (μV)	Latency (ms)
Condition I—No scar; probe on nerve (contralateral, unscarred side)	0.09	~1962	1.25
Condition II—Scar present; probe beside scar (≤1 mm lateral, scarred side)	0.10[a]	1891–2007	1.25

Condition I (no scar) was assessed on the contralateral unscarred side of the same animal, serving as a within-animal control. Condition II (scar present) was assessed on the ipsilateral scarred side. Data represent single recording sessions at each current level. [a] Side difference in threshold = 0.01 mA (scarred vs. unscarred side). The scarred side was Grade 1 (mild) per the scheme defined in the Surgical Exposure of the RLN subsection. Stimulation adjacent to the scar (≤1 mm lateral) produced only marginal threshold elevation without latency change, consistent with the limited insulating effect of small-volume fibrosis when the probe is placed on adjacent unscarred tissue (bilateral paradigm). These data represent the bilateral comparison performed in Series 2 animal B01. Two additional Series 2 animals (B02, B04) underwent an independent sequential within-site comparison (pre- vs. post-scar-dissection at the same stimulation site under stepped-current sampling from 0.05 to 2.0 mA). Those data are provided in **Supplementary Table 1a,b** and showed directionally consistent findings. The remaining four Series 2 animals (B03, B05–B07) were pre-specified for other experimental arms and did not undergo scar-vs-unscarred comparison. RLN, recurrent laryngeal nerve.

effect of scar as an electrical barrier to probe-delivered stimulation at off-nerve placements, whereas the sequential paradigm (B02, B04) captures the effect of scar on the nerve's local electrophysiological response to on-nerve stimulation. Both paradigms are reported because together they correspond to the two principal intraoperative circumstances in which peri-neural scar degrades EMG-based nerve monitoring.

The remaining four Series 2 animals (B03, B05–B07) did not undergo scar-vs-unscarred comparison. Animal B02, in addition to contributing the left-RLN sequential within-site scar-vs-unscarred data described above (**Supplementary Table 1a**), also underwent bilateral array-guided localization at the same Series 2 session (the Array-Guide Localization Procedure). Animals B05, B06, and B07 underwent array-guided localization at their Series 2 session (the Array-Guide Localization Procedure) but did not undergo scar-vs-unscarred comparison. Animal B03 was reserved at its Series 2 session for a separate exploratory protocol whose data are not reported in this manuscript, and subsequently contributed array-guided localization data at its Series 3 session.

Array-Guide Localization Procedure

Array-guide localization was evaluated in 9 rabbits (18 operated sides). Across the 18 sides, 450 stimulation sites in total were delivered (25 sites per 5 × 5 grid × 18 sides), and 90 row-level electrophysiological reference points (ERPs) were assessed for localization accuracy (5 transverse rows per side × 18 sides). Localization was performed under a skin-incision-only condition: after skin incision and superficial blunt dissection to reach the pretracheal fascia, the array guide was applied directly to the soft tissue overlying the expected RLN course without further dissection or nerve exposure. The operator advanced the stimulation probe through each numbered site (1–25) sequentially (Fig. 2B) at an initial mapping current of 0.5 mA in all animals, consistent with both the established clinical lower-bound for intraoperative nerve mapping (the Effective Stimulation Distance: Preliminary Experiment) and the empirically derived effective-radius/inter-site-spacing matching condition at this current (the Effective Stimulation Distance: Preliminary Experiment and the Results, Effective Stimulation Distance and Array Parameter Rationale). When no positive response was obtained at scarred sites in second- or third-operation animals, rescue stimulation at 0.8–1.0 mA was subsequently performed to determine whether the initial negative result was attributable to scar-related impedance. Peak amplitude and latency were recorded at each site.

The array was applied with its long axis aligned to the craniocaudal direction and its short axis spanning the paratracheal soft tissue between the trachea medially and the carotid sheath laterally. Within this fixed orientation, Col 5 (the most medial column) overlies the expected paratracheal location of the RLN in the tracheoesophageal groove, Col 2 overlies the expected position of the VN within the carotid sheath, and Col 1 (the most lateral column) overlies the lateral aspect of the carotid sheath. Because vagal stimulation produces an EMG response that is electrophysiologically indistinguishable from RLN stimulation but does not localize the RLN, and because the 1–2 mm effective stimulation radius at 0.5 mA (the Effective Stimulation Distance: Preliminary Experiment) suggests that stimulation from Col 1 may also recruit the VN within the carotid sheath, ERP candidacy was prospectively restricted by methodological design to Col 3, Col 4, and Col 5. Accordingly, Col 1 and Col 2 were excluded from ERP selection regardless of their measured EMG amplitudes. Within this Col 3–5 search window, a site was classified as positive when its EMG am-

plitude was ≥100 µV. In each transverse row (perpendicular to the trachea), the positive site within Col 3–Col 5 yielding the highest amplitude was designated the electrophysiological reference point (ERP) for that row, indicating the closest proximity to the RLN trunk. The nerve course was reconstructed by connecting the five consecutive row-level ERPs along the craniocaudal axis. After completing array-guide mapping and prior to array removal, the row-level electrophysiological reference points (ERPs) identified during the mapping pass were transferred onto the underlying paratracheal soft tissue by applying a small dot of sterile surgical marker ink through the corresponding 0.5 mm stimulation portal of the array. This step preserved the ERP coordinates on the tissue surface during subsequent dissection. The array was then removed, the strap muscles were further retracted as needed, and the RLN was surgically exposed in the tracheoesophageal groove to reveal its actual anatomical position. The perpendicular distance from each ERP mark to the closest point on the surgically exposed nerve trunk was measured at the time of surgery using a calibrated stainless-steel surgical ruler (1 mm graduations, practical resolution ±0.5 mm). Localization accuracy was defined as ERP-to-nerve distance ≤2 mm and was reported as a binary classification (≤2 mm vs. >2 mm) rather than as a continuous distance. The 2-mm threshold was selected as both a clinically meaningful spatial bound for nerve localization and a value safely above the resolution of conventional ruler measurement, such that the binary classification is robust to ordinary measurement uncertainty. All distance measurements were performed intraoperatively by the same operator to maintain consistency. Formal inter-observer reliability of the measurement was not assessed in this pilot study and is acknowledged as a limitation in the Discussion. Following completion of array-guide localization and subsequent surgical exposure of the RLN, the thickness of the soft tissue layer overlying the nerve at the midpoint of the array guide footprint was measured with a calibrated surgical ruler in each animal and on each side. These measurements were recorded to characterize the tissue interposition depth under the skin-incision-only condition and to contextualize the effective stimulation distance data presented in the Effective Stimulation Distance: Preliminary Experiment.

Statistical Analysis

This study was designed as an exploratory pilot investigation. Electrophysiological amplitude data are therefore presented primarily as raw values, ranges, or representative recordings rather than subjected to formal hypothesis-driven comparisons.

For localization performance, the primary analytical unit was the operated side rather than the individual stimulation site, because the five row-level electrophysiological reference points (ERPs) obtained from the same side were not statistically independent. Per-side localization accuracy was calculated as the proportion of accurate ERPs among the five transverse rows on each side. These per-side accuracy values were summarized descriptively across the 18 operated sides. Site-level accuracy (accurate ERPs/all ERPs) is additionally reported as a descriptive measure to facilitate intuitive interpretation of mapping performance, but these observations should not be interpreted as statistically independent. Accordingly, no formal inferential comparison based on site-level independence was considered the primary analysis. Any site-level side-to-side comparisons are presented for descriptive purposes only. Given the pilot nature of the study and limited sample size, formal subgroup comparisons among first-, second-, and third-operation groups were not performed. Proportions were calculated manually; descriptive statistics were computed and tabulated using SPSS 26.0 (IBM, Armonk, NY, USA); no inferential hypothesis testing was performed.

Results

Stimulation Thresholds of the RLN and Vagus Nerve

Threshold characterization was performed in the August 2024 cohort (representative animals: B01, B03, B04). Individual amplitude-versus-current profiles are presented in Table 1 and Fig. 3A. The RLN threshold ranged from 0.08 to 0.20 mA across the three animals, with plateau onset occurring between 0.10 and 0.30 mA and plateau amplitudes spanning 800–1782 µV across recording sessions (Table 1). The VN threshold was 0.10–0.30 mA, with plateau onset at 0.30–0.40 mA. As specified in the recording protocol (the Materials and Methods, Stimulation Threshold of the RLN and Vagus Nerve), all reported threshold and plateau amplitude data were obtained from the right RLN and right VN. Left-side RLN recording was attempted only in animal B04. Notably, one animal (B04) showed a substantially lower threshold on the left RLN (0.05 mA) accompanied by anomalously low plateau amplitude (278–324 µV). As detailed in the Materials and Methods (Stimulation Threshold of the RLN and Vagus Nerve) and the Table 1 footnote, this pattern is most consistent with suboptimal electrode-to-vocal cord contact at this recording site rather than intrinsic nerve pathology, supported by the normal plateau amplitude observed on the contralateral right RLN of the same animal (1065–1782 µV). The left-side session was therefore excluded from the threshold-amplitude profile under the pre-specified ≥500 µV quality criterion.

Critically, at 0.5 mA, the working current selected for the array guide, all tested RLNs and VNs produced plateau-level amplitudes (typically >1000 µV), confirming reliable and consistent neural activation. Across the tested current range (0.1–1.0 mA), signal latency showed no apparent variation in any animal (all recorded values within 1.20–1.30 ms), consistent with the established conduction properties of myelinated motor fibers. Formal statistical testing was not performed given the pilot nature of this study and the limited observation count.

Effective Stimulation Distance and Array Parameter Rationale

The preliminary stimulation distance experiment (the Materials and Methods, Effective Stimulation Distance: Preliminary Experiment) yielded the following results, which directly determined the final array design parameters. The effective stimulation distance increased markedly with current intensity (Fig. 3B). At 0.5 mA, only sites within 1–2 mm of the nerve surface produced positive EMG responses, yielding high spatial resolution. Within individual animal recordings, the empirical amplitude maximum at 0.5 mA did not always occur at the geometric 0-mm position. Modest sub-millimetre off-axis positions occasionally produced equal or marginally higher responses, consistent with near-threshold recruitment of motor fascicles distributed at varying depths and lateral positions beneath the nerve surface (Fig. 3B, upper panel). This per-animal positional sensitivity was attenuated at 1.0 mA (Fig. 3B, lower panel), where the distance-amplitude relationship exhibited a monotonic decrease with distance in each animal. These cohort-level effective-stimulation-radius conclusions are based on the four Series 1 animals (B02–B05) whose recording sessions met the pre-specified plateau-amplitude quality criterion (the Materials and Methods, Effective Stimulation Distance: Preliminary Experiment). At 1.0 mA, the effective distance extended to 4–5 mm, which would cause cross-activation between sites spaced 2 mm apart and substantially reduce the ability to discriminate nerve position.

These data directly justify the array guide design parameters: a 2-mm inter-point spacing fully exploits the 1–2 mm effective radius at 0.5 mA (no blind zones, no cross-activation), while a working current of 0.5 mA provides the best balance between reliable activation and spatial specificity. Under the skin-incision-only condition, positive EMG responses were successfully recorded at sites overlying the RLN course in all animals. The measured soft tissue thickness overlying the nerve ranged from 2.5 to 5.0 mm across all sides (mean 3.8 mm), indicating that the intervening tissue layer at this depth did not preclude signal acquisition at 0.5 mA. However, a formal quantitative comparison of EMG amplitude between the nerve-exposed and skin-incision-only conditions was not performed, and the degree of signal attenuation attributable to soft tissue interposition remains to be characterized.

Effect of Peri-Neural Scar Tissue on Electrophysiological Parameters

Gross anatomical examination revealed progressive peri-neural fibrosis across the three surgical groups (Fig. 4A–C), graded according to the four-point ordinal scheme defined in the Surgical Exposure of the RLN subsection. First-operation animals uniformly exhibited pristine anatomical planes with no scar-nerve contact (Grade 0, Fig. 4A). Second-operation animals (absorbable sutures, ~1-month interval) showed filmy scar contacting <25% of the nerve circumference, easily separable by blunt dissection (Grade 1, Fig. 4B). Third-operation animals (non-absorbable buried sutures, ~2-month cumulative interval) exhibited scar tissue involving an estimated 25–75% of the nerve circumference and required sharp dissection, although tissue planes remained identifiable and the nerve was not completely encased by scar tissue (Grade 2, Fig. 4C). Grade 3 (dense circumferential encasement) was not achieved in any animal in this study, consistent with the Limitations discussed in the Discussion.

Across the three Series 2 animals in which a scar-vs-unscarred electrophysiological comparison was performed (B01, B02, B04), three directionally consistent findings were observed regardless of the comparison paradigm. Specifically, the stimulation threshold required to evoke a reliable EMG response was elevated at scarred sites, response amplitudes at matched supra-threshold currents were reduced at scarred sites, and response latencies were prolonged at scarred sites. Quantitative data for the primary bilateral comparison (B01) are presented in Table 2. Data for the two independent sequential within-site comparisons (B02, B04) are presented in **Supplementary Table 1a,b**, with a cross-animal summary in **Supplementary Table 1c**. In B01, peri-neural fibrosis at the time of surgery was Grade 1 (mild; the Surgical Exposure of the RLN subsection scoring scheme), with no segment scar completely encircling the nerve (Table 2). When the stimulation probe was placed on unscarred tissue ≤1 mm lateral to the mildly scarred nerve segment, threshold was 0.10 mA compared with 0.09 mA on the contralateral unscarred side (difference 0.01 mA), and latency remained 1.25 ms in both conditions. These findings suggest that small-volume peri-neural fibrosis produces only marginal impedance elevation. The electrophysiological effect of dense circumferential scar tissue encasing the nerve could not be evaluated in this animal due to insufficient scar formation. Further investigation in animals with more advanced fibrosis will be required.

These findings have a direct practical implication for the array guide method: 0.5 mA is sufficient for patients in first-operation; however, in re-operative cases where scar tissue overlies the nerve, the working current should be increased to 0.8–1.0 mA to compensate for scar impedance. At these higher currents, the effective stimulation radius extends beyond the 2-mm inter-site spacing, such that multiple adjacent sites may simultaneously elicit positive responses. Under these conditions, the electrophysiological reference point must be identified by selecting the highest-amplitude site within each transverse row rather than by the presence of a unique positive site, as discussed further in the Discussion.

RLN Localization Accuracy of the Array Guide

Array-guide localization was evaluated once per animal in 9 rabbits, contributing 18 operated sides and 90 row-

Table 3. Descriptive site-level localization accuracy of the array-guide method.

Stage	Animals (n)	Sides (n)	ERPs (n)	Accurate at initial 0.5 mA mapping pass (n, %)	Recovered on rescue at 0.8–1.0 mA (n)	Final post-rescue accuracy (n, %)
First-operation	2	4	20	20 (100.0%)	0	20 (100.0%)
Re-operative (second- or third-operation)	7	14	70	63 (90.0%)	7	70 (100.0%)
Overall	9	18	90	83 (92.2%)	7	90 (100.0%)

Array-guided localization was performed once per animal, at a single surgical timepoint that depended on the animal's experimental endpoint within the longitudinal repeated-surgery design (the Experimental Animals subsection and Fig. 1). Two animals contributed array-guided localization data at their first operation (B08, B09; both reached experimental endpoint before Series 2). Four animals contributed at their second operation (B02, B05, B06, B07; reached endpoint before Series 3). Three animals contributed at their third operation (B01, B03, B04). Accuracy was defined as ERP-to-RLN distance ≤2 mm. Site-level proportions are presented for descriptive interpretation only. Because multiple ERPs were clustered within the same side and animal, these observations should not be interpreted as statistically independent, and no inferential subgroup testing between stages was performed (see the Statistical Analysis subsection). Within the re-operative group, all seven initially-false-negative ERPs at 0.5 mA were recovered on rescue stimulation at 0.8–1.0 mA, yielding a final post-rescue accuracy of 100% in both stage groups and overall. The re-operative animals included both second-operation animals (mild peri-neural fibrosis, Grade 1) and third-operation animals (moderate peri-neural fibrosis, Grade 2). See the Results (Effect of Peri-Neural Scar Tissue on Electrophysiological Parameters) and Fig. 4 for the gross anatomical correlates. ERP, electrophysiological reference point; RLN, recurrent laryngeal nerve.

level electrophysiological reference points (ERPs) in total. The surgical timepoint at which the array procedure was performed depended on each animal's experimental endpoint within the longitudinal repeated-surgery design (the Experimental Animals subsection and Fig. 1). Two animals contributed array data at the first operation, four at the second operation, and three at the third operation (see Table 3 footnote for animal allocation). Because ERPs obtained from the same side are clustered observations, localization performance was summarized primarily at the side level. Across the 18 operated sides, the array guide consistently reconstructed the RLN trajectory, and the per-side proportion of accurate ERPs was high overall.

At the initial 0.5 mA mapping pass, 83 of 90 ERPs (92.2%) were within 2 mm of the surgically exposed RLN, which served as the anatomical reference standard. All seven initially-false-negative ERPs occurred in re-operative animals (Table 3) and were recovered on rescue stimulation at 0.8–1.0 mA at the same array footprint, yielding a final post-rescue site-level accuracy of 100%. Stratified by operative stage (Table 3), first-operation animals (n = 2) achieved 100% accuracy at the initial 0.5 mA pass with no rescue required, and re-operative animals (second- or third-operation, n = 7) achieved 90.0% accuracy at the initial pass and 100% after rescue. These stage-stratified proportions are reported for descriptive interpretation only, and no formal inferential testing between stages was performed, consistent with the pre-specified exploratory analytical posture (the Statistical Analysis subsection).

All seven initial-pass false-negative ERPs co-localized with grossly identifiable peri-neural scar tissue as confirmed at subsequent surgical exposure. No false-negative ERP occurred at an unscarred position on any side. A representative example from animal B01 at the third-operation time point (right side, August 2024 mapping session) is shown in Fig. 5B–D. Notably, the same animal also contributed data to the second-operation cohort presented in the Results (Effect of Peri-Neural Scar Tissue on Electrophysiological Parameters) and Table 2. The array-guide localization data shown here were derived from the subsequent third-operation session. Widespread false-negative responses at 0.5 mA co-localized with the scarred region (Fig. 5B) were fully reversed on rescue stimulation at 1.0 mA at the same array footprint, with all row-wise ERPs recovered within 2 mm of the surgically exposed RLN (Fig. 5C,D). The spatial concordance between false-negative sites and the scarred region, together with the reversibility of the negative response by modest current elevation, is most parsimoniously explained by scar-related impedance attenuating current delivery at 0.5 mA rather than by array-guide misplacement or intrinsic nerve dysfunction.

Visualization of the RLN Course

By marking positive sites on the array grid and connecting consecutive electrophysiological reference points (ERPs) longitudinally as a continuous red dashed trajectory (Fig. 5), the RLN course was reconstructed in all 18 operated sides. In the majority of animals, ERPs aligned along the tracheoesophageal groove in a craniocaudal direction, closely matching the anatomically confirmed nerve path. Representative localization maps from a second-operation animal (B05) and a third-operation animal (B01) are shown in Fig. 5A and Fig. 5B–D, respectively. At 0.5 mA, where the array footprint in B05 overlay a paratracheal region away from the filmy peri-neural scar present at this animal's Grade 1 surgical stage (the Results, Effect of Peri-Neural Scar Tissue on Electrophysiological Parameters),

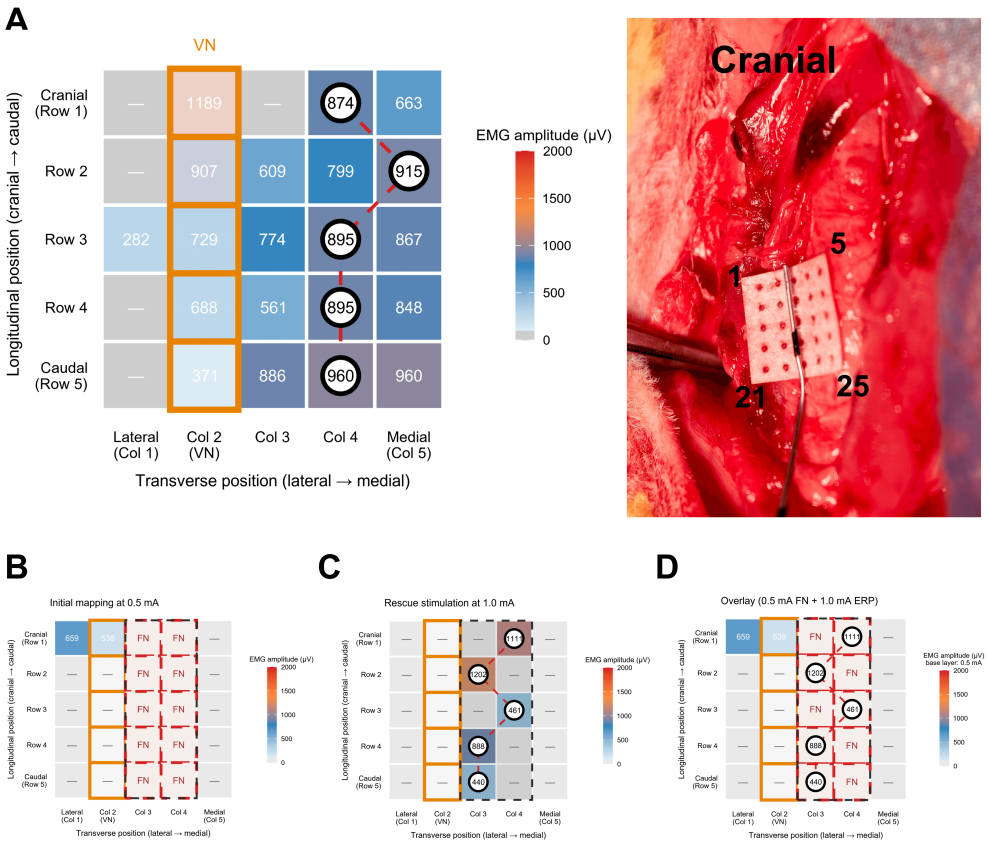

Fig. 5. Recurrent laryngeal nerve (RLN) localization and course visualization using the array guide. Representative localization maps from two animals selected to illustrate different stages of peri-neural scar severity. (A) Localization map from a second-operation animal (rabbit B05; Grade 1 peri-neural fibrosis; the Results, Effect of Peri-Neural Scar Tissue on Electrophysiological Parameters) at 0.5 mA, with the array footprint placed at a paratracheal region away from the scarred nerve segment. The corresponding intraoperative photograph shows the array guide applied to the paratracheal soft tissue (sites 1, 5, 21, 25 numbered for orientation). (B–D) Representative maps from a third-operation animal with denser peri-neural scar (rabbit B01, right side). The hatched grey region delineates the gross extent of peri-neural scar tissue documented at subsequent surgical exposure. (B) At the initial 0.5 mA mapping pass, the majority of sites within the scarred region failed to elicit a positive EMG response (red dashed squares labelled FN). The row-wise electrophysiological reference points (ERPs) were not definable in this pass, and the RLN trajectory was therefore not drawn. (C) On rescue stimulation at 1.0 mA at the same array footprint, all five row-wise ERPs were recovered, and the reconstructed RLN trajectory is shown as a red dashed line connecting consecutive ERPs along the craniocaudal axis. (D) Overlay of B and C. Red dashed squares mark sites that were false-negative at 0.5 mA, black circles mark the ERPs recovered at 1.0 mA, and the red dashed line again traces the reconstructed RLN trajectory. The spatial concordance between false-negative sites and the scarred region, together with the reversibility of the negative response by modest current elevation, supports the interpretation that scar-related impedance, rather than array-guide misplacement, accounted for the false-negative responses. Each grid is displayed with Row 1 (cranial) at the top and Row 5 (caudal) at the bottom. Columns are arranged with Col 1 on the left (overlying the lateral aspect of the carotid sheath) and Col 5 on the right (overlying the medial paratracheal soft tissue immediately adjacent to the trachea). The orange border marks Col 2, which, under the standard array placement used in this study, overlies the VN within the carotid sheath. Col 1 was positioned lateral to the VN over the lateral wall of the sheath. The fill color of Col 2 was visually de-emphasized with a semi-transparent overlay because vagal stimulation does not localize the RLN, and Col 2 was therefore excluded from ERP selection by methodological design (Section the Array-Guide Localization Procedure). Grey tiles with an em-dash denote sub-threshold sites (<100 μV), and no grid position is left blank. Black circles mark row-wise ERPs, defined as the site with the maximum EMG amplitude within each row, evaluated across Col 3–5 only. Red dashed lines connect consecutive ERPs along the craniocaudal axis to depict the reconstructed RLN trajectory. This line is shown in (A,C,D) but is intentionally omitted in (B), where the 0.5 mA initial pass produced widespread scar-related false-negatives and row-wise ERPs were not reliably definable until the rescue stimulation shown in (C). EMG, electromyographic; ERP, electrophysiological reference point; FN, false-negative; RLN, recurrent laryngeal nerve; VN, vagus nerve. Rabbit B01 contributes data at multiple surgical time points in this study. The localization mapping shown in (B–D) was performed at its third operation (August 2024).

the strongest responses were observed at sites directly overlying the nerve (within 1 mm), while sites 2 mm away (e.g., Col 4 relative to Col 5) also produced positive responses of lower amplitude, consistent with the 1–2 mm effective stimulation radius established in the Results (Effective Stimulation Distance and Array Parameter Rationale) and Fig. 3B. In one animal, the right-sided RLN was found to follow an anomalous lateral course toward the carotid sheath at surgical exposure. The corresponding ERP cluster and the red dashed trajectory connecting them shifted laterally along the craniocaudal axis, accurately reconstructing the aberrant trajectory without prior anatomical assumption.

Discussion

The present study describes the design, parameter optimization, and initial validation of a surface matrix electrode array guide for nerve-unexposed, multi-point electrophysiological mapping of the RLN in a rabbit model. The central finding is that a structured 5 × 5 stimulation grid, operated at an empirically determined working current of 0.5 mA with 2-mm inter-site spacing, can reconstruct the RLN course as a continuous electrophysiological trajectory without mandatory nerve exposure, achieving a site-level localization accuracy of 92.2% under a skin-incision-only condition (Table 3). These findings address a practical gap in current intraoperative neuromonitoring practice: whereas conventional intermittent IONM provides point-by-point electrophysiological confirmation at surgeon-selected locations, it does not generate a systematic spatial map of the nerve's course, a limitation that becomes particularly consequential in the re-operative field where anatomical landmarks are distorted by fibrosis and the nerve may be substantially displaced from its expected position [12,24].

Intraoperative neuromonitoring has become a widely adopted, and in many centers routine, adjunct in thyroid surgery; it helps identify otherwise unrecognized RLN dysfunction intraoperatively and has been associated with lower rates of postoperative RLN injury/vocal cord dysfunction, particularly by guiding staged surgery after loss of signal [9,25]. However, conventional (intermittent) IONM relies on hand-held, sequential stimulation at discrete time points, providing site-specific electrophysiological feedback rather than continuous, image-based visualization of the nerve's full course [10,26]. With conventional intermittent IONM, the surgeon must integrate sequential, site-specific stimulation responses with the operative anatomy to localize the RLN trajectory; this process is surgeon-dependent and may be time-consuming, particularly in re-operative fields where scar tissue, fibrosis, and nerve displacement obscure normal landmarks [15,27].

The array-guide method addresses these limitations by replacing sequential freehand exploration with a structured, reproducible 5 × 5 stimulation grid. By applying the guide to the paratracheal soft tissue and advancing the probe through each of the 25 numbered sites, the operator generates a spatial amplitude map in a single, systematic pass. Positive sites are identified by amplitude threshold (≥100 μV), and the nerve course is reconstructed by connecting the highest-amplitude site in each transverse row, the electrophysiological reference point (ERP), along the craniocaudal axis. This approach converts an otherwise abstract electrophysiological signal into an explicit, reproducible anatomical map.

Compared with existing multi-point mapping strategies, the array-guide method offers several practical distinctions. The stimulating dissector and intermittent freehand probing require the operator to manually direct each stimulation event toward a suspected nerve location, an approach that remains operator-dependent and provides no systematic spatial coverage of the operative field. Continuous IONM detects traction-related injury in real time but is not designed for pre-dissection localization. The array guide, by contrast, covers a defined 10 × 10 mm tissue area in a single structured pass, generating a spatial amplitude map without requiring prior knowledge of nerve position. This property is particularly relevant in re-operative fields, where normal anatomical landmarks are absent, and the nerve may be substantially displaced, as illustrated by the variant course identified in one animal in the present study.

It should be emphasized that the array-guide method is positioned as a complementary, region-specific adjunct to conventional intermittent IONM rather than as a replacement for it. The 10 × 10 mm flexible array is designed for pre-dissection topographic localization of the RLN along its paratracheal mid-cervical segment, where the tissue contour is approximately planar at the scale of the array footprint and where landmark-based identification is most prone to error in the re-operative setting. The array is not intended for use at the laryngeal entry zone, the cricothyroid joint and the immediately adjacent Berry's ligament region, where the nerve transitions to a vertical insertion course, the surgical field narrows, and the local anatomy becomes sharply non-planar. In these distal zones, the conventional handheld monopolar probe retains its essential role, both because of its unconstrained spatial flexibility and because the operative field by this stage of dissection typically permits direct visual identification of the nerve. Matrix electrode arrays previously deployed on larger and flatter biological surfaces, such as the cardiac epicardium and the cortical surface, illustrate the general principle that planar arrays perform best on planar tissue. The present design applies that principle to a smaller and shallower planar region of cervical soft tissue, not to all surgical zones of the neck.

A related question concerns the applicability of the present design to endoscopic and robotic thyroid surgery, which now account for a substantial and growing fraction of contemporary practice. The array described in this

study is engineered for direct application through an open midline cervical incision, and direct deployment through trocar-based or transoral approaches is not feasible without re-engineering. Three principal adaptations would be required. The 10 × 10 mm planar footprint exceeds the working diameter of typical 5–12 mm endoscopic trocars and would require a foldable or rollable substrate capable of *in-situ* deployment within the working space, analogous to mesh delivery in laparoscopic hernia repair. Also, the loss of natural soft-tissue compression in CO_2-insufflated working spaces would require an actively conformable substrate or a temporary anchoring mechanism to ensure reliable electrode-tissue apposition. Moreover, for robotic platforms, the array could be designed for direct manipulation by a robotic grasper, with the 25-point stimulation sweep automated under console control. In our view, this is the most attractive long-term translational pathway, because console automation simultaneously addresses both the deployment and the operator-dependence limitations identified for the open application. The array footprint may also need to be reduced (for example, to a 3 × 3 grid spanning 6 × 6 mm) for narrow-port compatibility, with the inter-site spacing re-derived under the geometric constraints set out in the Materials and Methods (Effective Stimulation Distance: Preliminary Experiment). None of these adaptations have been empirically validated in the present study, and the applicability of the method to endoscopic and robotic thyroid surgery should be regarded as a directed future engineering and validation program rather than an immediate clinical claim of the present manuscript.

A critical design question for any multi-point stimulation array is the trade-off between spatial resolution and reliable signal acquisition. If the inter-site spacing is too large relative to the effective stimulation radius, blind zones exist between adjacent sites and the nerve may be missed. If the working current is too high, the effective radius expands to the point where adjacent sites cross-activate each other, degrading spatial specificity.

Our preliminary experiments empirically resolved this trade-off. At 0.5 mA, positive responses were confined to sites within 1–2 mm of the nerve surface, yielding an effective stimulation radius that precisely matches the 2-mm inter-site spacing of the array: every point within the grid falls within the effective radius of at least one adjacent site, eliminating blind zones, while the radius is small enough to prevent cross-activation. At 1.0 mA, the effective radius extended to 4–5 mm, which would cause simultaneous activation of multiple non-adjacent sites spaced 2 mm apart and substantially reduce the ability to identify the closest site to the nerve. These data support the use of 0.5 mA as the working current in first-operation cases and confirm the selection of 2-mm inter-site spacing for the array design at this current level. We additionally note that the empirically observed sub-millimetre offset between the geometric 0 mm position and the per-animal amplitude maximum at 0.5 mA (Fig. 3B, upper panel) does not undermine the array-guide method, because the operational definition of the electrophysiological reference point within each transverse row is the highest-amplitude site within the row rather than the site closest in absolute geometric terms to a presumed nerve location. This offset lies well within the 2 mm inter-site spacing and 2 mm localization-accuracy criterion used in the present study and is therefore absorbed by the existing methodological definition rather than constituting a confound.

Perineural scarring and fibrosis in the re-operative thyroid bed, as encountered in thyroid re-operations, represent one of the most challenging settings for RLN identification because prior surgery distorts tissue planes, displaces the nerve, and obscures normal anatomical landmarks [12,24]. Scar tissue in re-operative thyroid fields may increase the effective electrical impedance and attenuate current delivery to the RLN, thereby increasing the stimulation threshold required to elicit a suprathreshold EMG response and raising the risk of false-negative mapping if the working current is not adjusted accordingly [28,29].

In our second-operation animal (B01), mild perineural fibrosis (Grade 1 per the scheme defined in the Surgical Exposure of the RLN subsection, filmy scar contacting <25% of the nerve circumference, with no segment fully encircling the nerve) elevated the stimulation threshold by only 0.01 mA relative to the contralateral unscarred side (0.10 vs. 0.09 mA), and latency was unchanged at 1.25 ms in both conditions. These findings indicate that small-volume peri-neural fibrosis exerts minimal insulating effect and does not require substantial current modification. By contrast, in second- and third-operation animals with denser scar, the seven initially false-negative sites (7.8% of total) were recovered by increasing the working current to 0.8–1.0 mA (Table 3), suggesting that scar-related impedance, rather than array misplacement, accounted for these initial failures. At 0.8–1.0 mA, the effective stimulation radius extends beyond the 2-mm inter-point spacing, meaning that multiple adjacent sites may simultaneously elicit positive EMG responses. Under these conditions, the ERP identification strategy must rely on relative amplitude discrimination rather than an absolute threshold criterion: within each transverse row, the site producing the highest amplitude is still expected to represent the closest proximity to the nerve, because current density, and therefore EMG amplitude, decreases monotonically with distance from the nerve surface. While this approach preserves the ability to identify the most probable nerve location even at higher currents, the spatial precision is inherently lower than at 0.5 mA, and the 2-mm localization accuracy criterion used in this study may be more difficult to achieve consistently. Based on these findings, we tentatively propose 0.5 mA as the standard working current for primary operations and 0.8–1.0 mA for re-operative cases, as detailed in the Results (Effect of Peri-Neural Scar Tissue on Electrophysiological

Parameters). It should be emphasized that the adequacy of this strategy under conditions of dense circumferential fibrosis remains to be established and will require evaluation in a dedicated large-animal model.

It should be noted that the scar model employed in this study produced predominantly mild-to-moderate perineural fibrosis. The electrophysiological performance of the array-guide method under dense, circumferential scar encasement, as frequently encountered in complex human re-operations, could not be fully evaluated and represents an important area for future investigation (see the limitations discussed in the Discussion).

One animal in the present study exhibited a right-sided RLN course variant, and the precise nature of this variant (congenital displacement versus non-recurrent course) could not be determined from the present data and warrants further characterization. Crucially, the array-guide positive-site cluster shifted correspondingly, accurately reflecting the aberrant course without any prior anatomical knowledge or assumption. Although the precise variant type in this animal was not definitively classified, the observation illustrates a clinically important property of the array-guide method. Because localization is driven entirely by the spatial EMG amplitude pattern rather than fixed anatomical assumptions, the method retains its inferential capability regardless of whether the nerve follows its typical course. This property is relevant to a spectrum of anatomical variants encountered clinically, ranging from lateral or medial positional displacement to the rare non-recurrent laryngeal nerve (reported in approximately 0.5–1.0% of right-sided operations [30,31,32]), all of which are associated with an elevated surgical risk precisely because they deviate from conventional landmark-based anatomical expectations. Because the array-guide method generates an unbiased spatial amplitude map rather than guiding the operator toward a presumed anatomical location, it retains localization capability in the presence of variant anatomy, a feature that purely landmark-based or single-point approaches cannot reliably provide.

Several limitations of this study should be acknowledged. First, and most critically, the fibrosis model employed produced predominantly mild-to-moderate perineural adhesion; dense circumferential encasement of the RLN, representative of the most challenging human re-operative scenarios, was not achieved in any animal. Whether the current-adjustment strategy (0.8–1.0 mA) remains adequate under maximal scar encasement is the most important unresolved question for clinical translation and is designated as the primary objective of future large-animal work with a dedicated dense-fibrosis model. Additionally, the rabbit RLN differs substantially from the human RLN in nerve caliber, anatomical course, depth from the skin surface, and surrounding soft tissue composition. The present findings therefore cannot be directly extrapolated to clinical practice without further validation in a large-animal model with cervical anatomy more closely approximating that of the human, or in human cadaveric specimens. Also, the total sample size was limited to nine animals, of which only three completed the third-operation series. This limits the statistical power, precludes formal subgroup comparisons between surgical groups, and prevents calculation of precise confidence intervals for localization accuracy. Fourth, the precise degree of EMG signal attenuation attributable to soft tissue interposition under the skin-incision-only condition was not formally quantified and remains a priority for future large-animal characterization. Furthermore, the array guide was fabricated manually in this study. Standardization of fabrication processes, sterilization protocols, and mechanical properties will be required before clinical translation, and the dimensions may need to be modified to accommodate the larger anatomical scale of the human neck. In addition, the planar geometry of the array limits its applicability to regions where the tissue surface is approximately planar at the 10×10 mm scale of the array footprint. The array is not suitable for use at the laryngeal entry zone, where the nerve transitions to a vertical insertion course and the local anatomy is sharply non-planar, nor in surgical fields too narrow to accommodate the full array footprint. In these regions, conventional handheld probe-based intermittent IONM remains the appropriate modality, and the array-guide method should be regarded as a complementary, region-specific adjunct rather than a general substitute. Future iterations incorporating reduced footprints, segmental or modular array architecture, or actively conformable substrates may extend applicability to a wider range of surgical zones. A further limitation concerns the precision of the localization accuracy outcome itself. Because the perpendicular ERP-to-nerve distance was measured intraoperatively with a conventional surgical ruler (1 mm graduations, practical resolution ±0.5 mm), absolute distances cannot be reported at sub-millimeter precision in this study. The categorical 2 mm threshold used to classify ERPs as accurate or inaccurate was selected partly with this measurement-resolution consideration in mind, and is robust to ordinary ruler-based measurement error. Nevertheless, formal precision-recall characterization at sub-millimeter spatial resolution will require higher-precision measurement modalities, such as calibrated stereoscopic photogrammetry, intraoperative high-frequency ultrasound, or imaging-correlated spatial registration, in future large-animal validation work. Inter-observer reliability of the distance measurement was likewise not formally assessed in the present pilot study. Moreover, the scar-vs-unscarred electrophysiological comparison was performed in three of the seven Series 2 animals (B01, B02, B04), and the remaining four animals were pre-specified for other experimental arms of the study. Although the two paradigms used (bilateral in B01, sequential within-site in B02 and B04) yielded directionally concordant findings, the paradigms differ methodologically, and the absolute magnitudes are therefore not

directly comparable across animals. A larger, methodologically uniform study with graded fibrosis severities will be required to formally quantify the electrophysiological impact of peri-neural scar on intraoperative EMG-based laryngeal nerve monitoring.

Future work should focus on four areas. First, validation in a large-animal model (e.g., porcine or ovine) with cervical anatomy more representative of humans will be essential before clinical trials can be designed. This validation should additionally incorporate higher-precision measurement of the ERP-to-nerve distance to enable continuous-distance reporting and formal sub-millimeter precision-recall characterization beyond the binary 2 mm criterion used in the present pilot study. Second, development of a dedicated scar model with dense circumferential peri-neural fibrosis will enable systematic characterization of the current-adjustment strategy required in the most demanding re-operative scenarios. Third, integration of automated sequential stimulation, eliminating the need for manual probe advancement through each of the 25 sites, would further reduce localization time and operator variability, and represents the most impactful engineering advance for clinical translation in the open-surgery setting. In addition, adaptation of the array geometry, substrate, and deployment mechanism to endoscopic and robotic thyroid surgery represents a parallel engineering pathway that, if successful, would extend the method to the substantial and growing fraction of thyroid procedures performed via minimally invasive approaches. The specific design adaptations required for this pathway are outlined earlier in this section.

Conclusions

This study presents the design, parameter optimization, and proof-of-concept validation of a surface matrix electrode array guide for nerve-unexposed RLN mapping in a New Zealand White rabbit model. By empirically establishing that a 2-mm inter-site spacing and a working current of 0.5 mA provide the optimal balance between spatial resolution and reliable neural activation, the array guide demonstrated a localization accuracy of 92.2% across 90 sites under a skin-incision-only condition, providing initial evidence for the feasibility of the method, with no clinically meaningful asymmetry between left and right sides. The method successfully reconstructed the RLN course as a continuous electrophysiological trajectory in every animal tested, including one case of anatomical course variation, without reliance on fixed positional assumptions. A pragmatic current-adjustment strategy (0.8–1.0 mA) was identified to compensate for scar-related impedance in the mild-to-moderate fibrosis range modelled in this study; its adequacy under dense circumferential peri-neural encasement remains to be established. Taken together, these preliminary findings demonstrate that the array-guide method may be feasible, reproducible, and spatially informative for pre-dissection localization of the RLN along its paratracheal mid-cervical segment, offering a structured, region-specific complement to conventional single-point IONM exploration rather than a replacement for it. Further validation in large-animal models and human cadaveric or early translational settings will be required before clinical application can be considered.

Availability of Data and Materials

The data that support the findings of this study are available from the corresponding author upon reasonable request.

Author Contributions

JLW and XHC designed the research study. WQH and TL performed the research. JH and FWT analyzed the data. JLW drafted the article. All authors contributed to important editorial changes in the manuscript. All authors gave final approval of the version to be published. All authors have participated sufficiently in the work and agreed to be accountable for all aspects of the work.

Ethics Approval and Consent to Participate

The study was approved by the Institutional Animal Care and Use Committee of Laboratory Animal Sciences, Chinese Academy of Medical Sciences (approval no. KR-IACUC-T-2024-011). All procedures complied with the ARRIVE Guidelines 2.0.

Acknowledgment

We sincerely thank all laboratory staff for their dedicated efforts throughout this study. We are also grateful to the Institute of Automation, Chinese Academy of Sciences for its technical assistance in the research.

Funding

This work was supported by “Yangfan” Program Clinical Technology Innovation Project (Medical-Engineering Integration Cultivation Project) (Beijing Hospitals Authority, Grant No. YGLH202504).

Conflict of Interest

The authors declare no conflict of interest.

Supplementary Material

Supplementary material associated with this article can be found, in the online version, at https://doi.org/10.24976/Discov.Med.202638210.175.

References

[1] Al-Hakami H, Al Garni M. Incidence and risk factors for recurrent laryngeal nerve injury after thyroid surgery. The Egyptian Journal of Otolaryngology. 2024; 40: 92. https://doi.org/10.1186/s43163-024-00655-9

[2] Liao LJ, Wang CT. Management of Unilateral Vocal Fold Paralysis after Thyroid Surgery with Injection Laryngoplasty: State of Art Review. Frontiers in Surgery. 2022; 9: 876228. https://doi.org/10.3389/fsurg.2022.876228

[3] Titulaer K, Schlattmann P, Guntinas-Lichius O. Surgery for bilateral vocal fold paralysis: Systematic review and meta-analysis. Frontiers in Surgery. 2022; 9: 956338. https://doi.org/10.3389/fsurg.2022.956338

[4] Gunn A, Oyekunle T, Stang M, Kazaure H, Scheri R. Recurrent Laryngeal Nerve Injury After Thyroid Surgery: An Analysis of 11,370 Patients. The Journal of Surgical Research. 2020; 255: 42–49. https://doi.org/10.1016/j.jss.2020.05.017

[5] Jung JY. Intraoperative Nerve Monitoring in Thyroid Surgery: A Comprehensive Review of Technical Principles, Anesthetic Considerations, and Clinical Applications. Journal of Clinical Medicine. 2025; 14: 3259. https://doi.org/10.3390/jcm14093259

[6] Chen BY, Stack BC. Methods of Recurrent Laryngeal Nerve Monitoring. In Scharpf J, Randolph GW (eds.) Intraoperative Cranial Nerve Monitoring in Otolaryngology-Head and Neck Surgery (pp. 73–82). Springer International Publishing: Cham. 2022. https://doi.org/10.1007/978-3-030-84916-0_7

[7] Priya S, Garg S, Dandekar M. Intraoperative monitoring of the recurrent laryngeal nerve in surgeries for thyroid cancer: a review. Journal of Cancer Metastasis and Treatment. 2021; 7: 70. https://doi.org/10.20517/2394-4722.2021.122

[8] Wojtczak B, Sutkowska-Stępień K, Głód M, Kaliszewski K, Sutkowski K, Barczyński M. Current Knowledge on the Use of Neuromonitoring in Thyroid Surgery. Biomedicines. 2024; 12: 675. https://doi.org/10.3390/biomedicines12030675

[9] Hearn M, You B, Mady LJ, Frazier KM, Morris-Wiseman L, Mathur A. Progress and Outcomes of Intraoperative Nerve Monitoring During Thyroidectomy. JAMA Otolaryngology– Head & Neck Surgery. 2025; 151: 236–242. https://doi.org/10.1001/jamaoto.2024.4452

[10] McManus C, Kuo JH. Intraoperative Neuromonitoring: Evaluating the Role of Continuous IONM and IONM Techniques for Emerging Surgical and Percutaneous Procedures. Frontiers in Endocrinology. 2022; 13: 808107. https://doi.org/10.3389/fendo.2022.808107

[11] Sun H, Tian W, Chinese Thyroid Association, College of Surgeons, Chinese Medical Doctor Association; Chinese Research Hospital Association Thyroid Disease Committee. Chinese guidelines on intraoperative neuromonitoring in thyroid and parathyroid surgery (2023 edition). Gland Surgery. 2023; 12: 1031–1049. https://doi.org/10.21037/gs-23-284

[12] Gumus S, Yuksel C, Pulat H, Akyuz C, Gul MO. Inferior-to-Superior Dissection for Recurrent Laryngeal Nerve Identification in Redo Thyroid Surgery: Enhanced Safety and Reduced Injuries. Journal of Clinical Medicine. 2024; 13: 7364. https://doi.org/10.3390/jcm13237364

[13] Russell MD, Kamani D, Randolph GW. Intraoperative nerve monitoring in surgery for thyroid cancer. Annals of Thyroid. 2020; 5: 18. https://doi.org/10.21037/aot-20-42

[14] Yao XY, Li X, Yu B, Liu SR, Wang BY, Lu SY, et al. Ultrasound Visualization of the Recurrent Laryngeal Nerve: A Prospective Clinical Validation Study. Annals of Surgical Oncology. 2025; 32: 1309–1316. https://doi.org/10.1245/s10434-024-16529-6

[15] Karaisli S, Gucek Haciyanli S, Haciyanli M. Comparison of stimulating dissector and intermittent stimulating probe for the identification of recurrent laryngeal nerve in reoperative setting. European Archives of Oto-rhino-laryngology : Official Journal of the European Federation of Oto-Rhino-Laryngological Societies (EUFOS) : Affiliated with the German Society for Oto-Rhino-Laryngology - Head and Neck Surgery. 2022; 279: 443–447. https://doi.org/10.1007/s00405-021-06801-w

[16] Barczyński M. Laryngeal Nerves Monitoring in Thyroid Surgery. In Testini M, Gurrado A (eds.) Thyroid Surgery (pp. 113–122). Springer International Publishing: Cham. 2024. https://doi.org/10.1007/978-3-031-31146-8_12

[17] Kirke DN, Sinclair CF. Recurrent Laryngeal Nerve Monitoring: Nuts and Bolts. Otolaryngologic Clinics of North America. 2024; 57: 53–61. https://doi.org/10.1016/j.otc.2023.08.002

[18] He Y, Li Z, Yang Y, Lei J, Peng Y. Preoperative Visualized Ultrasound Assessment of the Recurrent Laryngeal Nerve in Thyroid Cancer Surgery: Reliability and Risk Features by Imaging. Cancer Management and Research. 2021; 13: 7057–7066. https://doi.org/10.2147/CMAR.S330114

[19] Nouh MR, Abdel-Naby HM, El Sakka T, El-Shafei M. Peripheral nerve ultrasound: a survival guide for the practicing radiologist with updates. The Ultrasound Journal. 2025; 17: 21. https://doi.org/10.1186/s13089-024-00387-0

[20] Lee D, Yu HW, Kim S, Yoon J, Lee K, Chai YJ, et al. Vision-based tracking system for augmented reality to localize recurrent laryngeal nerve during robotic thyroid surgery. Scientific Reports. 2020; 10: 8437. https://doi.org/10.1038/s41598-020-65439-6

[21] Li B, Wei H, Yan J, Wang X. A novel portable augmented reality surgical navigation system for maxillofacial surgery: technique and accuracy study. International Journal of Oral and Maxillofacial Surgery. 2024; 53: 961–967. https://doi.org/10.1016/j.ijom.2024.02.007

[22] Lee E, Lee K, Yu HW, Kim SJ, Chai YJ, Choi JY, et al. Comparison of Recurrent Laryngeal Nerve Identification Time in the Lower Central Triangle during Thyroid Surgery Using Neurophysiological Mapping and Monitoring. Medicina (Kaunas, Lithuania). 2021; 57: 748. https://doi.org/10.3390/medicina57080748

[23] Puanhvuan D, Chumnanvej S, Wongsawat Y. Electrical stimulation-based nerve location prediction for cranial nerve VII localization in acoustic neuroma surgery. Brain and Behavior. 2018; 8: e00981. https://doi.org/10.1002/brb3.981

[24] Medas F, Tuveri M, Canu GL, Erdas E, Calò PG. Complications after reoperative thyroid surgery: retrospective evaluation of 152 consecutive cases. Updates in Surgery. 2019; 71: 705–710. https://doi.org/10.1007/s13304-019-00647-y

[25] Wilhelm A, Conroy PC, Calthorpe L, Frye W, Sosa JA, Roman S. Routine use of intraoperative nerve monitoring is associated with a reduced risk of vocal cord dysfunction after thyroid cancer surgery. BMC Surgery. 2023; 23: 215. https://doi.org/10.1186/s12893-023-02122-3

[26] Gibson MM, Chen AY. Intermittent Neuromonitoring of the Recurrent Laryngeal and Vagus Nerves: the Ins and Outs. Current Otorhinolaryngology Reports. 2021; 9: 316–325. https://doi.org/10.1007/s40136-021-00351-9

[27] Cirillo B, Brachini G, Cavallaro G, Tarallo M, Carlino C, Duranti G, et al. The Application of Intermittent Intraoperative Neuromonitoring (I-IONM) and Continuous Intraoperative Neuromonitoring (C-IONM) During Thyroid Surgery: A Single-Center Study. Journal of Clinical Medicine. 2025; 14: 2612. https://doi.org/10.3390/jcm14082612

[28] Wojtczak B, Sutkowski K, Kaliszewski K, Barczyński M, Bolanowski M. Thyroid reoperation using intraoperative neuromonitoring. Endocrine. 2017; 58: 458–466. https://doi.org/10.1007/s12020-017-1443-x

[29] Lotti F, Ranieri F, Vadalà G, Zollo L, Di Pino G. Invasive Intraneural Interfaces: Foreign Body Reaction Issues. Frontiers

in Neuroscience. 2017; 11: 497. https://doi.org/10.3389/fnins.2017.00497

[30] Liddy W, Wu CW, Dionigi G, Donatini G, Giles Senyurek Y, Kamani D, et al. Varied Recurrent Laryngeal Nerve Course Is Associated with Increased Risk of Nerve Dysfunction During Thyroidectomy: Results of the Surgical Anatomy of the Recurrent Laryngeal Nerve in Thyroid Surgery Study, an International Multicenter Prospective Anatomic and Electrophysiologic Study of 1000 Monitored Nerves at Risk from the International Neural Monitoring Study Group. Thyroid : Official Journal of the American Thyroid Association. 2021; 31: 1730–1740. https://doi.org/10.1089/thy.2021.0155

[31] So JTK, Thompson CSG. Non-Recurrent Laryngeal Nerve: Surgical Risk of Injury in Comparison With the Normal Recurrent Laryngeal Nerve-A Systematic Review and Meta-Analysis. Clinical Otolaryngology : Official Journal of ENT-UK ; Official Journal of Netherlands Society for Oto-Rhino-Laryngology & Cervico-Facial Surgery. 2025; 50: 654–663. https://doi.org/10.1111/coa.14312

[32] Henry BM, Sanna S, Graves MJ, Vikse J, Sanna B, Tomaszewska IM, et al. The Non-Recurrent Laryngeal Nerve: a meta-analysis and clinical considerations. PeerJ. 2017; 5: e3012. https://doi.org/10.7717/peerj.3012